

Pairing interactions and pairing mechanism in high temperature copper oxide superconductors

Guo-meng Zhao*

Department of Physics and Astronomy, California State University, Los Angeles, CA 90032, USA

The polaron binding energy E_p in undoped parent cuprates has been determined to be about 1.0 eV from the unconventional oxygen-isotope effect on the antiferromagnetic ordering temperature. The deduced value of E_p is in quantitative agreement with that estimated from independent optical data and that estimated theoretically from the measured dielectric constants. The substantial oxygen-isotope effect on the in-plane supercarrier mass observed in optimally doped cuprates suggests that polarons are bound into the Cooper pairs. We also identify the phonon modes that are strongly coupled to conduction electrons from the angle-resolved photoemission spectroscopy, tunneling spectra, and optical data. We consistently show that there is a very strong electron-phonon coupling feature at a phonon energy of about 20 meV along the antinodal direction and that this coupling becomes weaker towards the diagonal direction. We further show that high-temperature superconductivity in cuprates is caused by strong electron-phonon coupling, polaronic effect, and significant coupling with 2 eV Cu-O charge transfer fluctuation.

I. INTRODUCTION

Developing the microscopic theory for high- T_c superconductivity is one of the most challenging problems in condensed matter physics. Eighteen years after the discovery of the high- T_c cuprate superconductors by Bednorz and Müller¹, there have been no microscopic theories that can describe the physics of high- T_c superconductors completely and unambiguously. Due to the high T_c values and the observation of a small oxygen-isotope effect on T_c in a 90 K cuprate superconductor $\text{YBa}_2\text{Cu}_3\text{O}_{7-y}$ (YBCO)²⁻⁴, many theorists believe that the electron-phonon interaction is not important in bringing about high- T_c superconductivity. Most physicists have thus turned their minds towards alternative pairing interactions of purely electronic origin.

On the other hand, there is overwhelming evidence that electron-phonon coupling is very strong in the cuprate superconductors⁵⁻²⁰. In particular, various unconventional oxygen-isotope effects Zhao and his coworkers have observed since 1994 clearly indicate that the electron-phonon interactions are so strong that polarons/bipolarons are formed in doped cuprates^{5-9,11,12,14-17,19} and manganites^{21,22}, in agreement with a theory of high-temperature superconductivity²³ and the original motivation for the discovery of high-temperature superconductivity¹. However, such clear experimental evidence for strong electron-phonon interactions from the unconventional isotope effects has been generally ignored. In the 2001 Nature paper¹⁸, Lanzara *et al.* appear to provide evidence for strong coupling between doped holes and the 70 meV half-breathing phonon mode from angle-resolved photoemission spectroscopy (ARPES). They further show that this 70 meV phonon mode can lead to d-wave pairing symmetry and is mainly responsible for high-temperature superconductivity²⁴. Very recently, Devereaux *et al.*²⁵ have proposed that the 40 meV B_{1g}

phonon mode rather than the 70 meV half-breathing phonon mode is responsible for d-wave high-temperature superconductivity. This pairing mechanism contradicts the very recent ARPES data, which show that multiple phonon modes at 27 meV, 45 meV, 61 meV, and 75 meV are strongly coupled to doped holes in deeply underdoped $\text{La}_{2-x}\text{Sr}_x\text{CuO}_4$ ²⁰. The strong coupling to the multiple phonon modes is not in favor of d-wave gap symmetry but may support a general s-wave gap symmetry^{26,27}.

Here we determine the polaron binding energy E_p for undoped parent cuprates from the unconventional oxygen-isotope effect on the antiferromagnetic ordering temperature (T_N)⁵. The determined value (~ 1.0 eV) of E_p is in quantitative agreement with that estimated from independent optical data²⁸ and that estimated theoretically from the measured dielectric constants²⁹. The substantial oxygen-isotope effect on the in-plane supercarrier mass observed in optimally doped cuprates^{6,17,19} indicates that polarons are bound into the Cooper pairs. We also identify the phonon modes that are strongly coupled to conduction electrons from the angle-resolved photoemission spectroscopy, tunneling spectra, and optical data. We consistently show that there is a very strong electron-phonon coupling feature at a phonon energy of about 20 meV along the antinodal direction and that this coupling becomes weaker towards the diagonal direction. We further show that high-temperature superconductivity in cuprates is caused by strong electron-phonon coupling, polaronic effect, and significant coupling with 2 eV Cu-O charge transfer fluctuation.

II. OXYGEN-ISOTOPE EFFECT ON T_N IN LA_2CUO_4

The antiferromagnetic order (AF) observed in the parent insulating compounds like La_2CuO_4 signals a strong electron-electron Coulomb correlation. On the other

hand, if there is a very strong electron-phonon coupling such that the Migdal adiabatic approximation breaks down, one might expect that the antiferromagnetic exchange energy should depend on the isotope mass. Following this simple argument, Zhao and his co-workers initiated studies of the oxygen isotope effect on the AF ordering temperature in several parent compounds in 1992. A noticeable oxygen-isotope shift of T_N was consistently observed in La_2CuO_4 .⁵

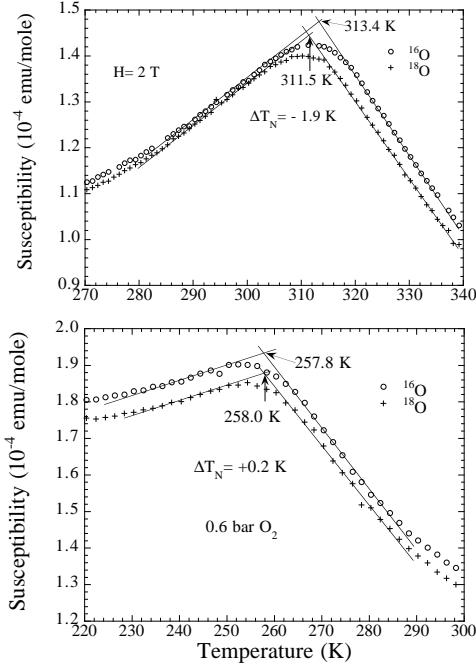


FIG. 1. The temperature dependence of the susceptibility for the ^{16}O and ^{18}O samples of the undoped La_2CuO_4 (upper panel), and of the oxygen-doped $\text{La}_2\text{CuO}_{4+y}$ (lower panel). After⁵.

Fig. 1 shows the temperature dependence of the susceptibility for the ^{16}O and ^{18}O samples of undoped La_2CuO_4 (upper panel), and of oxygen doped $\text{La}_2\text{CuO}_{4+y}$ (lower panel). One can see that the AF ordering temperature T_N for the ^{18}O sample is lower than the ^{16}O sample by about 1.9 K in the case of the undoped samples. For the oxygen-doped samples, there is a negligible isotope effect.

It is known that the antiferromagnetic properties of $\text{La}_2\text{CuO}_{4+y}$ can be well understood within mean-field theory which leads to a T_N formula³⁰:

$$k_B T_N = J' [\xi(T_N)/a]^2, \quad (1)$$

where J' is the interlayer coupling energy, $\xi(T_N)$ is the in-plane AF correlation length at T_N with $\xi(T_N) \propto \exp(J/T_N)$ for $y = 0$ (J is the in-plane exchange energy). When T_N is reduced to about 250 K by oxygen

doping, a mesoscopic phase separation has taken place so that $\xi(T_N) = L$ (Ref.³¹), where L is the size of the antiferromagnetically correlated clusters, and depends only on the extra oxygen content y . In this case, we have $T_N = J'(L/a)^2$. Since L is independent of the isotope mass, a negligible isotope shift of T_N in the oxygen-doped $\text{La}_2\text{CuO}_{4+y}$ suggests that J' is independent of the isotope mass. Then we easily find for undoped compounds

$$\Delta T_N/T_N = (\Delta J/J) \frac{B}{1+B}, \quad (2)$$

where $B = 2J/T_N \simeq 10$. From the measured isotope shift of T_N for the undoped samples, we obtain $\Delta J/J \simeq -0.6\%$.

Recently, Eremin *et al.*³² have considered strong electron-phonon coupling within a three-band Hubbard model. They showed that the antiferromagnetic exchange energy J depends on the polaron binding energy E_p^O due to oxygen vibrations, on the polaron binding energy E_p^{Cu} due to copper vibrations, and on their respective vibration frequencies ω_O and ω_{Cu} . At low temperatures, J is given by³²

$$J = J_c \left(1 + \frac{3E_p^O \hbar \omega_O}{\Delta_{pd}^2} + \frac{3E_p^{Cu} \hbar \omega_{Cu}}{\Delta_{pd}^2} \right). \quad (3)$$

Here Δ_{pd} is the charge-transfer gap, which is measured to be about 1.5 eV in undoped cuprates. The oxygen-isotope effect on J can be readily deduced from Eq. 3:

$$\frac{\Delta J}{J} = \left(\frac{3E_p^O \hbar \omega_O}{\Delta_{pd}^2} \right) \left(\frac{\Delta \omega_O}{\omega_O} \right). \quad (4)$$

Substituting the unbiased parameters $\hbar \omega_O = 0.075$ eV, $\Delta J/J \simeq -0.6\%$, $\Delta_{pd} = 1.5$ eV, and $\Delta \omega_O/\omega_O = 6.0\%$ into Eq. 4, we find that $E_p^O = 1.0$ eV. The total polaron binding energy should be larger than 1.0 eV since E_p^{Cu} should not be zero. The parameter-free estimate of the polaron binding energy due to the long-range Fröhlich-type electron-phonon interaction has been made for many oxides including cuprates and manganites²⁹. The total polaron binding energy for La_2CuO_4 was estimated to be about 1 eV (Ref.²⁹), in excellent agreement with the value deduced above from the isotope effect. The polaron binding energy can be also estimated from optical data where the energy of the mid-infrared peak E_m in the optical conductivity is equal to $2\gamma E_p$ (Ref.²⁹), where γ is 0.2–0.3 (Ref.²⁹). The peak position E_m was found to be about 0.6 eV for $\text{La}_{1.98}\text{Sr}_{0.02}\text{CuO}_4$ (Ref.²⁸), implying that $E_p = 1.0$ –1.5 eV. This is in quantitative agreement with the value estimated from the isotope effect. These results thus consistently suggest that the polaron binding energy of undoped La_2CuO_4 is about 1 eV. Doping will reduce the value of E_p and thus E_m due to screening of charged carriers. The optical conductivity data indeed show that $E_m = 0.44$ eV and 0.12 eV for $x = 0.06$ and 0.15, respectively²⁸.

One may argue that the mid-infrared peak could arise from magnetic excitations. A sharp peak feature at about 0.35 eV was seen in the optical conductivity of the undoped $\text{YBa}_2\text{Cu}_3\text{O}_6$ (Ref.³³). This feature was also seen in other undoped cuprates^{34,35}, and can be well explained by the phonon assisted two magnon excitation³⁵. However, this sharp feature is very different from a broad peak at about 0.6 eV in lightly doped $\text{La}_{1.98}\text{Sr}_{0.02}\text{CuO}_4$. In particular, the maximum conductivity for the two magnon peak is about $1 (\Omega^{-1}\text{cm}^{-1})$ ³³⁻³⁵, which is over two orders of magnitude lower than that for the broad peak in $\text{La}_{1.98}\text{Sr}_{0.02}\text{CuO}_4$ (Ref.³⁶). Therefore, the broad peak in doped $\text{La}_{1.98}\text{Sr}_{0.02}\text{CuO}_4$ cannot have the same origin as the sharp peak in the undoped system.

III. OXYGEN-ISOTOPE EFFECT ON THE IN-PLANE SUPERCARRIER MASS

One of the most remarkable oxygen-isotope effects we have observed is the oxygen-isotope effect on the penetration depth^{6-9,14-17,19}. We made the first observation of this effect in optimally doped $\text{YBa}_2\text{Cu}_3\text{O}_{6.93}$ in 1994⁶. By precisely measuring the diamagnetic signals for the ^{16}O and ^{18}O samples, we were able to deduce the oxygen-isotope effects on the penetration depth $\lambda(0)$ and on the supercarrier density n_s . It turns out that $\Delta n_s \simeq 0$, and $\Delta\lambda(0)/\lambda(0) = 3.2\%$ (Ref.⁶). These isotope effects thus suggest that the effective supercarrier mass depends on the oxygen-isotope mass.

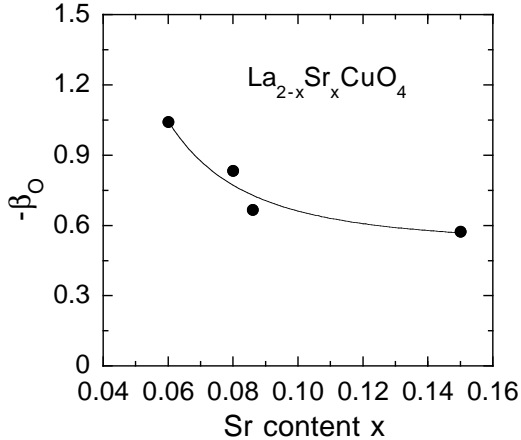


FIG. 2. The doping dependence of the exponent (β_O) of the oxygen-isotope effect on the in-plane supercarrier mass in $\text{La}_{2-x}\text{Sr}_x\text{CuO}_4$. The exponent is defined as $\beta_O = -d\ln m_{ab}^{**}/d\ln M_O$. The data are from Ref.^{14,16,17}.

In fact, for highly anisotropic materials, the observed isotope effect on the angle-averaged $\lambda(0)$ is the same as the isotope effect on the in-plane penetration depth $\lambda_{ab}(0)$. From the magnetic data for $\text{YBa}_2\text{Cu}_3\text{O}_{6.93}$,

$\text{La}_{1.85}\text{Sr}_{0.15}\text{CuO}_4$, and $\text{Bi}_{1.6}\text{Pb}_{0.4}\text{Sr}_2\text{Ca}_2\text{Cu}_3\text{O}_{10+y}$, we found that $\Delta\lambda_{ab}(0)/\lambda_{ab}(0) = 3.2 \pm 0.7\%$ for the three optimally doped cuprates¹⁷. Several independent experiments have consistently shown that the carrier densities of the two isotope samples are the same within 0.0004 per unit cell^{8,9,15}. Therefore, we can safely conclude that the observed oxygen-isotope effect on the in-plane penetration depth is caused only by the isotope dependence of the in-plane supercarrier mass m_{ab}^{**} . Recently, direct measurements of the in-plane penetration depth by low energy muon-spin-relaxation (LE μ SR) technique¹⁹ have confirmed our earlier isotope-effect results. It was found that¹⁹ $\Delta\lambda_{ab}(0)/\lambda_{ab}(0) = 2.8 \pm 1.0\%$. It is remarkable that the isotope effect obtained from the most advanced technology (LE μ SR)¹⁹ is the same as that deduced from simple magnetic measurements^{6,17,19}.

Fig. 2 shows the doping dependence of the exponent (β_O) of the oxygen-isotope effect on the in-plane supercarrier mass in $\text{La}_{2-x}\text{Sr}_x\text{CuO}_4$. Here the exponent is defined as $\beta_O = -d\ln m_{ab}^{**}/d\ln M_O$ (where M_O is the oxygen mass). It is apparent that the exponent increases with decreasing doping, in agreement with the fact that doping reduces electron-phonon coupling due to screening. The large oxygen-isotope effect on the in-plane supercarrier mass cannot be explained within the conventional phonon-mediated pairing mechanism where the effective mass of supercarriers is independent of the isotope mass³⁷. In particular, the substantial oxygen-isotope effect on m_{ab}^{**} in optimally doped cuprates indicates that the polaronic effect is not vanished in the optimal doping regime where the BCS-like superconducting transition occurs. This suggests that polaronic carriers may be bound into the Cooper pairs in optimally doped and overdoped cuprates, in agreement with theory^{38,23,39}.

IV. STRONG ELECTRON-PHONON COUPLING FEATURES ALONG THE DIAGONAL DIRECTION

In conventional superconductors, strong electron-phonon coupling features can be identified from single-particle tunneling spectra. For high- T_c cuprates, high-quality tunneling spectra are difficult to obtain because of a short coherence length. Moreover, due to a strong gap anisotropy, the energies of the strong coupling features will depend on the tunneling directions. Only if one can make a directional tunneling, one may be able to accurately identify the electron-phonon coupling features from the tunneling spectrum. On the other hand, the observation of the electron self-energy renormalization effect in the form of a “kink” in the band dispersion may reveal coupling of electrons with phonon modes. The “kink” feature at an energy of about 65 meV has been seen in the band dispersion of various cuprate superconductors along the diagonal (“nodal”) direction¹⁸. From the measured dispersion, one can extract the real

part of the electron self-energy that contains information about coupling of electrons with collective boson modes. The remarkable progress in the ARPES experiments is that the fine electron-phonon coupling structures have been revealed in the high-resolution ARPES data of a Be surface⁴⁰. Very recently, such fine coupling structures have been also seen in the raw data of the electron self-energy of deeply underdoped $\text{La}_{2-x}\text{Sr}_x\text{CuO}_4$ along the diagonal direction²⁰. Using the maximum entropy method (MEM) procedure, they are able to extract the electron-phonon spectral density $\alpha^2F(\omega)$ that contains coupling features at 27 meV, 45 meV, 61 meV and 75 meV. The energies of these coupling features are one-to-one correspondences to the phonon energies measured by inelastic neutron scattering²⁰. These beautiful ARPES data and exclusive data analysis²⁰ clearly indicate that the phonons rather than the magnetic collective mode are responsible for the electron self-energy effect.

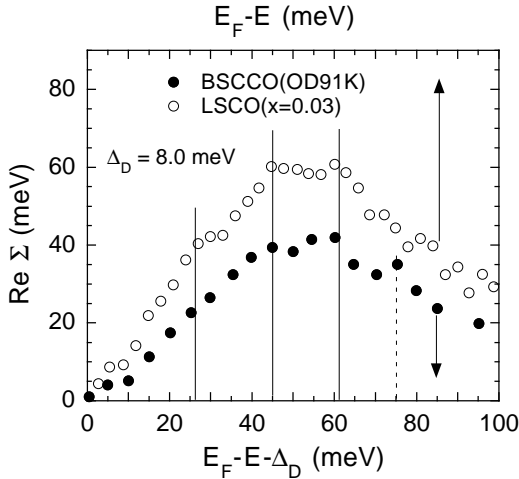


FIG. 3. The real part of the electron self-energy along the diagonal direction for a slightly overdoped BSCCO with $T_c = 91$ K (OD91K)⁴¹ and for $\text{La}_{2-x}\text{Sr}_x\text{CuO}_4$ with $x = 0.03$ (Ref.²⁰). The energy scale for BSCCO is shifted down by $\Delta_D = 8.0$ meV. The solid vertical lines at 27 meV, 45 meV, and 61 meV mark the energies of the pronounced phonon peaks in the electron-phonon spectral density $\alpha^2F(\omega)$ of $\text{La}_{1.97}\text{Sr}_{0.03}\text{CuO}_4$, which is determined from the MEM procedure²⁰. The dashed vertical line indicates the energy of an extra pronounced phonon peak (75 meV) in the superconducting LSCO with $x = 0.07$. It is interesting that the coupling feature at 27 meV in LSCO appears to shift to a lower energy of about 20 meV in BSCCO.

Here we will demonstrate that the fine coupling structures also appear in the earlier high-resolution ARPES data of a slightly overdoped BSCCO with $T_c = 91$ K (OD91K)⁴¹. Fig. 3 shows the real part of the electron self-energy along the diagonal direction for the OD91K sample at 70 K. In the same figure, we also plot the real part of the electron self-energy along the diagonal

direction for the nonsuperconducting $\text{La}_{2-x}\text{Sr}_x\text{CuO}_4$ (LSCO) with $x=0.03$. We can clearly see the fine structures in the raw data of both LSCO and BSCCO. The solid vertical lines mark the energies of the pronounced phonon peaks (27 meV, 45 meV, 61 meV) in the electron-phonon spectral density $\alpha^2F(\omega)$ of the nonsuperconducting $\text{La}_{1.97}\text{Sr}_{0.03}\text{CuO}_4$, which is determined from the MEM procedure²⁰. The dashed vertical line indicates the energy of an extra pronounced phonon peak (75 meV) in the superconducting LSCO with $x = 0.07$. In order for three pronounced fine structures (45 meV, 61 meV, and 75 meV) in the self-energy of BSCCO to be aligned with those for LSCO, the energy scale for BSCCO has to be shifted down by $\Delta_D = 8.0$ meV. This suggests that the superconducting gap along the diagonal direction is about 8 meV at 70 K. Using the BCS temperature dependence of the gap, one finds $\Delta_D = 10$ meV at zero temperature.

The finite superconducting gap of about 10 meV along the diagonal direction is consistent with a general s-wave gap symmetry (s + g wave) with eight line nodes ($g > s$)²⁶. This gap symmetry has double gap features at Δ_M and Δ_D in the superconducting density of states²⁶, which can be seen in the single-particle tunneling spectra and in the Andreev reflection spectra. Various break-junction spectra suggest that $\Delta_D = 9.5$ meV and $\Delta_M = 26$ meV in an overdoped BSCCO with $T_c = 89$ K (Ref.²⁶), $\Delta_D = 12 \pm 1$ meV and $\Delta_M = 24 \pm 1$ meV in an overdoped BSCCO with $T_c = 86$ K (Ref.⁴²), $\Delta_D = 7.5$ -9.0 meV and $\Delta_M = 15$ -18 meV in heavily overdoped BSCCOs with $T_c = 62$ K (Ref.^{43,44}). The Andreev reflection spectrum also indicates that $\Delta_D = 13$ meV in an overdoped BSCCO with $T_c = 85$ K (Ref.⁴⁵), while the other Andreev reflection spectrum shows a gap feature at $\Delta_M = 25$ meV (Ref.⁴⁶). Further, the Raman data⁴⁷ clearly indicate s + g wave gap symmetry in a heavily overdoped BSCCO with $T_c = 55$ K. The Raman intensities in both B_{1g} and B_{2g} symmetries increase linearly with energy up to $1.3\Delta_M$ and can be extrapolated to nearly zero values at zero energy. The linear energy dependence of the Raman intensity up to $1.3\Delta_M$ in the B_{1g} symmetry could be consistent with either clean s + g wave superconductivity⁴⁸ or very dirty d-wave superconductivity with $\sqrt{\Gamma\Delta_M(0)} \simeq 1.3\Delta_M$ (where Γ is the impurity scattering rate)⁴⁹. Very dirty d-wave superconductivity would give a significant residual intensity at zero energy⁴⁹, in disagreement with experiment⁴⁷. Very dirty d-wave superconductivity would also give a T^2 dependence of the in-plane penetration depth below $T^* = 0.83\sqrt{\Gamma\Delta_M(0)} \simeq 1.1\Delta_M \simeq 180$ K (Ref.⁵⁰), in contradiction with the observed linear- T dependence below 10 K⁵¹. In Ref.²⁶, the author has consistently explained all the relevant experiments in terms of the s + g wave gap symmetry and also shown that some phase sensitive experiments apparently supporting a d-wave order parameter symmetry do not contradict the s + g wave gap symmetry.

It is interesting to note that the coupling feature at

75 meV is invisible in the deeply underdoped LSCO ($x = 0.03$), but becomes pronounced in the superconducting LSCO ($x = 0.07$)²⁰ and in BSCCO (OD91K). This is consistent with the neutron experiments that clearly demonstrate that the coupling to the 75 meV half-breathing mode increases with increasing doping¹⁰. Further, the coupling feature at 27 meV in LSCO appears to shift to a lower energy of about 20 meV in BSCCO (see Fig. 3).

V. STRONG ELECTRON-PHONON COUPLING FEATURES ALONG THE ANTINODAL DIRECTION

The electron self-energy effect along the antinodal direction has been studied for several BSCCO crystals (OD91K, OD71K, and OD58K)⁵². The kink feature in the band dispersion or the peak feature in the electron self-energy along the antinodal direction is much stronger than that along the diagonal direction. This indicates a much stronger electron-boson coupling. One of the puzzling issues is that the energies of the boson modes shift to a much lower energy (about 20 meV) and are nearly independent of doping⁵². Fig. 4 shows the boson energy as a function of T_c for several overdoped BSCCO. The boson energy from the ARPES data is calculated according to $E_{boson} = E_{kink} - \Delta_M$, where E_{kink} is the kink energy in the band dispersion, which is found to be equal to the peak energy in the electron self-energy⁵². The above relation that is predicted by theory⁵³ was also used by the authors of Ref.⁵² to extract the mode energy. Since the antinodal gap Δ_M is found to be very close to the peak energy in the energy distribution curve (EDC)⁵⁴, one can simply take Δ_M being equal to the EDC peak energy. It is apparent that the boson energy is about 20 meV for heavily overdoped BSCCOs and about 16 meV for nearly optimally doped BSCCO. The strong coupling feature at about 20 meV also agrees with the electron-boson spectral density $\alpha^2F(\omega)$ deduced from a break-junction spectrum of BSCCO (OD93K)⁵⁵, as shown in Fig. 5. The spectral density clearly shows strong coupling features at about 20 meV, 36 meV, 60 meV, and 72 meV, similar to the features at about 20 meV, 62 meV, and 75 meV along the diagonal direction (see Fig. 3). Because the superconducting gap is very anisotropic, the excellent match of the phonon energies obtained from the tunneling spectrum and ARPES indicates that the tunneling process of this break-junction should be rather directional. Comparing the gap size of 23 meV determined from the spectrum⁵⁵ with the angle dependence of the gap^{54,26}, we find that the spectrum may mainly probe the superconducting density of states along the directions of between 10° and 20° from the antinodal direction. It is interesting that the strong coupling feature at 36 meV is only seen in the tunneling spectrum that mainly probes the states near the antinodal regime. The 36 meV phonon mode should be the oxygen buckling mode (B_{1g})

that has been shown to couple more strongly to the states near the antinodal direction²⁵. Such a strong angle dependence of the coupling strength may also occur to the other phonon modes such as the 45 meV mode that has a stronger coupling along the diagonal direction. What is more puzzling is that the band dispersion along the antinodal direction has a single kink feature associated with the 20 meV boson mode. A very likely explanation is that the phonon modes with energies higher than 30 meV lie below the bottom of the band continuum and thus the kink features for these modes disappear²⁵. Significantly away from the antinodal direction, the energies of all the modes are within the band continuum so the kink features for these modes will show up.

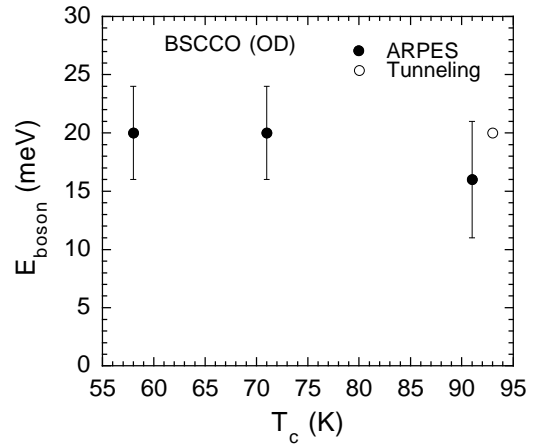


FIG. 4. The boson energy as a function of T_c for several overdoped BSCCO. The boson energy extracted from ARPES (Ref.⁵²) is calculated according to $E_{boson} = E_{kink} - \Delta_M$, where E_{kink} is the kink energy in the band dispersion, which is found to be equal to the peak energy in the electron self-energy⁵². One data point (open circle) is from the tunneling data (see Fig. 5).

The much stronger coupling to the 20 meV phonon modes along the antinodal direction is rather unusual. This is possible if the extended van Hove singularity is about 20 meV below the Fermi level and the electron-phonon matrix element for the 20 meV phonon modes has a maximum around $\vec{q} = 0$, where \vec{q} is the phonon wavevector. The large density of states at the van Hove singularity (20 meV below the Fermi level) and strong Fermi surface nesting along the antinodal direction greatly enhance the phase space available for 20 meV small- \vec{q} phonons to scatter quasiparticles from the states near the antinodal regime to the extended saddle points. The first principle calculation⁵⁶ indeed shows that unusual long-range Madelung-like interactions lead to very large matrix elements especially for zone center modes ($\vec{q} = 0$), which are mainly related to vibrations of cations (e.g., La, Sr, Ba, Ca). The phonon energies for the vibrations of the cations are between 15 meV to 25 meV (Ref.⁵⁶).

Since the strong coupling feature almost disappears above T_c , the 20 meV bosonic mode may be related to the magnetic resonance mode rather than the phonons. First, the energy of the bosonic mode is nearly independent of T_c (see Fig. 4) while the resonance energy is proportional to T_c (Ref.⁵⁷). This implies that the 20 meV boson is not the magnetic resonance mode. Second, the disappearance of the coupling feature above T_c does not necessarily mean that the coupling to the phonon modes is irrelevant. Very recent calculation²⁵ shows that the feature of coupling to the B_{1g} phonon mode (36 meV) is very weak in the normal state. As pointed out by these authors²⁵, the dramatic temperature dependence arises from a substantial change in the electronic occupation distribution and the opening of the superconducting gap. In the normal state, the phonon self-energy is a Fermi function at 100 K centered at the phonon energy, which results in a thermal broadening of $4.4k_B T$ or 38 meV, significantly larger than the phonon energy (20 meV). At low temperatures and in the superconducting state, the phonon self-energy is sharply defined due to the step-function-like Fermi function and a singularity in the superconducting density of states.

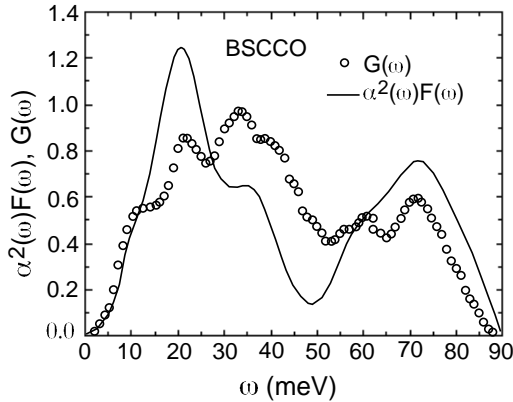


FIG. 5. The electron-phonon spectral density $\alpha^2 F(\omega)$ for a slightly overdoped $\text{Bi}_2\text{Sr}_2\text{CaCu}_2\text{O}_{8+y}$ (BSCCO) crystal, which was deduced from a break-junction spectrum⁵⁵.

Now we further show that a strong coupling feature in optical data, which was previously explained as due to a strong coupling between electrons and the magnetic resonance mode^{58,59}, is actually consistent with a strong electron-phonon coupling at a phonon energy of about 20 meV. It is known that the electron-phonon spectral density $\alpha^2 F(\omega)$ can be obtained through inversion of optical data. Marsiglio *et al.*⁶⁰ introduced a dimensionless function $W(\omega)$ which is defined as the second derivative of the normal state optical scattering rate $\tau^{-1}(\omega) = (\Omega_p^2/4\pi)\Re\sigma^{-1}(\omega)$ multiplied by frequency ω . Here Ω_p is the bare plasma frequency and $\sigma(\omega)$ the normal state optical conductivity. Specifically,

$$W(\omega) = \frac{1}{2\pi} \frac{d^2}{d\omega^2} \frac{\omega}{\tau(\omega)} \quad (5)$$

which follows directly from experiment. Marsiglio *et al.*⁶⁰ made the very important observation that within the phonon range $W(\omega) \simeq \alpha^2 F(\omega)$.

In the superconducting state, a phonon mode that is strongly coupled to electrons will appear at an energy of $2\Delta(\vec{k}) + \omega_{ph}$ (where ω_{ph} is the phonon energy), that is, the energies of the phonon structures shift up by the pair-breaking energy $2\Delta(\vec{k})$ ⁶¹. Because the 20 meV phonon modes are much more strongly coupled to the states near the antinodal regime and because there is a large quasi-particle density of states at the maximum gap edge, there must be a maximum at $2\Delta_M + \omega_{ph}$ in $W(\omega)$. For slightly overdoped BSCCO with $T_c = 90$ K, $\Delta_M = 26.0(5)$ meV (Ref.^{62,26}), so we should expect a maximum in $W(\omega)$ to be at about 72 meV. This is in quantitative agreement with the result shown in Fig. 6.

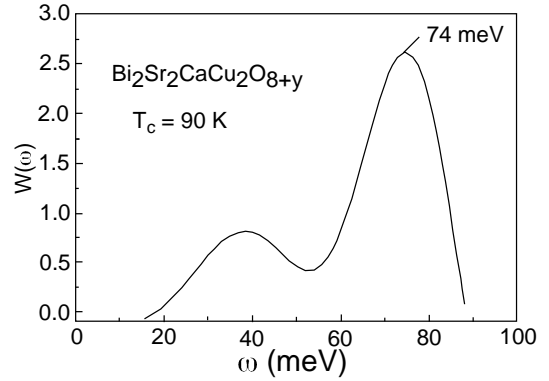


FIG. 6. The optically determined electron-boson spectral density $W(\omega)$ for a slightly overdoped BSCCO crystal with $T_c = 90$ K. After⁵⁹.

Recently, Devereaux *et al.* have calculated the electron-phonon interactions for the oxygen buckling mode (B_{1g}) and the in-plane half-breathing mode²⁵. They find that the 36 meV B_{1g} mode couples strongly to electronic states near the antinodal regime. They use an electron-phonon matrix element that is suitable only for $\text{YBa}_2\text{Cu}_3\text{O}_{7-y}$ where a large buckling distortion occurs. For other cuprates, the CuO_2 plane is flat and the buckling effect is negligible. Raman data have indeed shown that the coupling constant of the B_{1g} mode in BSCCO is more than one order of magnitude smaller than that in YBCO (Ref.⁶³). Even for YBCO, the coupling constant of this mode was deduced to be about 0.05 from the Raman data⁶³, in agreement with the earlier first principle calculation⁶⁴. Moreover, if this 40 meV phonon were strongly coupled to the electronic states near the antinodal regime, one would expect a maximum in $W(\omega)$ to occur at about 92 meV in slightly overdoped BSCCO with $T_c = 90$ K. This is in disagreement with experiment

(see Fig. 6).

Previously, the energy of the maximum in $W(\omega)$ was claimed to be in quantitative agreement with the theoretical prediction based on the strong coupling between electrons and the magnetic resonance mode^{58,59}. These authors^{58,59} argued that the maximum in $W(\omega)$ should occur at about $\Delta_M + E_r$, where E_r is the magnetic resonance energy. For BSCCO with $T_c = 90$ K, $\Delta_M = 26$ -28 meV and $E_r = 43$ meV, so one expects a maximum in $W(\omega)$ to occur at 69-71 meV, in reasonable agreement with the experimental result (see Fig. 6). Later on, more rigorous theoretical approach⁶⁶ shows that the maximum in $W(\omega)$ should occur at about $2\Delta_M + E_r$ rather than at $\Delta_M + E_r$. Then we should expect a maximum in $W(\omega)$ to occur at 96-98 meV, in disagreement with experiment.

If the maximum in $W(\omega)$ would occur at $\Delta_M + E_r$, the electron self-energy determined from the optical data would also have a maximum at $\Delta_M + E_r$. For the optimally doped BSCCO (OP96K) with $T_c = 96$ K, $\Delta_M = 37.5$ meV (Ref.⁶⁵), and E_r can be estimated to be 45 meV using the relation between E_r and T_c (Ref.⁵⁷). Then the maximum in the optically determined electron self-energy would occur at 82.5 meV. This predicted value is significantly lower than the measured one (96 meV)⁶⁷.

On the other hand, we can quantitatively explain the optically determined electron self-energy data in terms of the $s + g$ wave gap symmetry and electron-phonon coupling. Because the superconducting density of states have two sharp maxima at Δ_M and Δ_D for the $s + g$ gap symmetry²⁶, the optically determined electron self-energy should have two peak features, one at $2\Delta_M + E_1$ and another at $2\Delta_D + E_2$, where E_1 ($= 20$ meV) and E_2 are the averaged mode energies along the antinodal and diagonal directions, respectively. From Fig. 3, we find that $E_2 = 53$ meV, which is a simple average of the two pronounced peak energies (45 meV and 61 meV) in the electron self-energy. For OP96K, we predict two peak features at 95 meV and 73 meV in the optically determined electron self-energy. The predicted 73 meV peak feature will show up as a shoulder below the dominant peak feature at 95 meV. For an overdoped BSCCO with $T_c = 82$ K, $\Delta_M = 22$ -25 meV (Ref.^{42,65}) and $\Delta_D \simeq 12$ meV (see above), so two peak features will be located at 64-70 meV and 77 meV, respectively. For an overdoped BSCCO with $T_c = 60$ K, $\Delta_M = 14$ meV and $\Delta_D = 9$ meV (Ref.⁶⁸), so two peak features will show up at 48 meV and 71 meV, respectively. All these predicted peak features are in quantitative agreement with experiment⁶⁷.

It is interesting to note that the spectral density shown in Fig. 5 is extracted from a break-junction spectrum that has a clear dip feature at an energy of about 47 meV above the gap⁵⁵. The similar dip features are also seen in the ARPES spectra along the antinodal direction⁶⁹. In fact, the dip features of the superconducting density of states occur approximately at the valley energies and cut-off energy of the spectral density^{37,55,70}. For example, the cut-off energy of the spectral density for Pb is

about 9 meV (see Fig. 14 of Ref.³⁷) and the dip feature also occurs at 9 meV (see Fig. 14 of Ref.³⁷). On the other hand, if there is a single sharp peak in the spectral density, the dip feature will be slightly above the mode energy⁷¹. This implies that the dip energy measured from the gap is the upper limit of the mode energy. Because the peak features in the spectral density can be broadened by the strong coupling effect and disorder, the dip feature should shift to a higher energy towards the underdoping region where the coupling is much stronger⁶⁷. In the heavily overdoped region, the coupling is weak⁶⁷ and the peak width is narrow, so the dip energy is close to the mode energy. This can naturally explain why the dip energy of the UD70K sample is about 50 meV (Ref.⁷²), while the dip energy of the OD62K sample is about 24 meV (Ref.⁷²), which is slightly greater than the mode energy deduced from the electron self-energy above. In contrast, if one assumes that the dip energy measured from the gap is equal to the magnetic resonance energy, one cannot self-consistently explain the dip energy of 50 meV in the UD70K sample and of 28 meV in the OD87 K sample⁷³. The magnetic resonance energies for the UD70K and OD87K samples should be about 30 meV and 40 meV, respectively⁵⁷.

VI. STRONG COUPLING BETWEEN ELECTRONS AND CU-O CHARGE-TRANSFER EXCITATION.

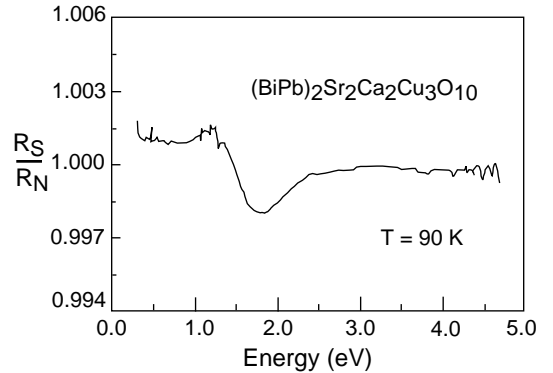


FIG. 7. The superconducting to normal-state reflectance ratio, R_s/R_N , for $(\text{BiPb})_2\text{Sr}_2\text{Ca}_2\text{Cu}_3\text{O}_{10}$ with $T_c = 105$ K. The figure is reproduced from⁷⁵.

In addition to strong electron-phonon interactions, there is a pronounced coupling feature at an energy of about 2 eV in the optical reflectance data^{74,75}. In Fig. 7, we plot the superconducting to normal-state reflectance ratio, R_s/R_N for $(\text{BiPb})_2\text{Sr}_2\text{Ca}_2\text{Cu}_3\text{O}_{10}$. It is clear that a strong coupling feature appears at about 2 eV. A similar strong coupling feature was also seen in YBCO, $\text{Tl}_2\text{Ba}_2\text{Ca}_2\text{Cu}_3\text{O}_{10}$, and $\text{Tl}_2\text{Ba}_2\text{Ca}_1\text{Cu}_2\text{O}_8$ (Ref.⁷⁵). Both the temperature and energy dependence

of the optical structure can be well described within Eliashberg theory with an electron-boson coupling constant of 0.30-0.35 (Ref.⁷⁵). Because the energy scale of this bosonic excitation is similar to the Cu-O charge transfer gap, it is likely that this high-energy bosonic mode corresponds to the Cu-O charge transfer excitation. A recent calculation based on three-band Hubbard model has indeed shown that the high energy Cu-O charge fluctuation can lead to a significant attractive interaction between conduction electrons and that the pairing symmetry is of extended s-wave (A_{1g})⁷⁶. The extended s-wave pairing symmetry is consistent with the conclusion²⁶ drawn from the comprehensive data analyses on nearly all the experiments that are used to test the gap symmetry.

VII. PAIRING MECHANISM

In two of our previous papers^{16,17}, we have proposed the pairing mechanism for optimally doped and overdoped cuprates. The long-range Fröhlich-type electron-phonon interaction and the short-range interaction of electrons with high-energy phonons lead to the formation of polarons. These interactions along with the coupling of electrons to the high-energy electronic excitations produce a negative value for the effective Coulomb pseudopotential μ^* . The polarons are bound into the Cooper pairs due to the negative μ^* and additional attractive interaction caused by the retarded electron-phonon interaction with the 20 meV phonon modes. The problem could then be solved within Eliashberg equations with an effective electron-phonon spectral density for the low-energy phonons and a negative Coulomb pseudopotential produced by the high-energy phonons and other high-energy bosonic excitations of purely electronic origin. Within this simplified approach, we are able to consistently explain the observed negligible isotope effect on T_c , substantial isotope effect on the supercarrier mass, large reduced energy gap, and high T_c value.

In this modified strong-coupling model, the effective electron-phonon coupling constant λ_{ep} for the low-energy phonons is enhanced by a factor of $f_p = \exp(g^2)$. Here $g^2 = A/\omega_H$, A is a constant, and ω_H is the frequency of the high-energy phonon mode¹⁷. The value of g^2 can be evaluated from the mid-infrared optical conductivity which exhibits a maximum at $E_m \simeq 0.12$ eV for optimally doped BSCCO⁷⁷ and LSCO²⁸. With $E_m = 0.12$ eV, $\hbar\omega_H = 75$ meV, we find $g^2 = E_m/(2\hbar\omega_H) = 0.8$, leading to $f_p = 2.2$.

From the spectral density shown in Fig. 5, we can extract the effective electron-phonon coupling constant λ_{ep} for the low-energy phonon mode, that is, $\lambda_{ep} \simeq 2.6$. If there were no polaronic mass enhancement, the coupling constant contributed from the low-energy phonons would be $2.6/f_p = 1.2$. With $\mu^* = 0.1$ and $\lambda_{ep} = 1.2$, we calculate $T_c = 18$ K according to a T_c formula⁷⁸

$$k_B T_c = 0.25 \hbar \sqrt{\langle \omega^2 \rangle} [\exp(2/\lambda_{eff}) - 1]^{-1/2}, \quad (6)$$

where

$$\lambda_{eff} = (\lambda_{ep} - \mu^*)/[1 + 2\mu^* + \lambda_{ep}\mu^*t(\lambda_{ep})], \quad (7)$$

The function $t(\lambda_{ep})$ is plotted in Fig. 2 of Ref.⁷⁸. In the present case, $\hbar\sqrt{\langle \omega^2 \rangle}$ is contributed only from the low-energy phonons and equal to 20 meV. Therefore, without the polaronic effect, T_c would not be higher than 20 K. On the other hand, with the polaronic effect, $\lambda_{ep} = 2.6$ and μ^* may be close to zero, leading to a T_c of about 54 K. Thus the polaronic effect enhances T_c significantly, but electron-phonon coupling alone cannot explain superconductivity above 100 K in optimally doped cuprates unless the polaronic effect can make $\mu^* < -0.15$.

In order to explain superconductivity above 100 K, it may be essential to consider the coupling to the high-energy electronic excitations. One of the high-energy excitations is the Cu-O charge transfer excitation at about 2 eV, as seen from the optical experiments^{74,75}. Since the high-energy phonon modes couple to electrons nonadiabatically, it is likely that the coupling of electrons to the 2 eV boson mode should also be nonadiabatic. Here we simply ignore the nonadiabaticity, and consider two δ -functions in the electron-boson spectral density to estimate T_c . One δ -function is at $\hbar\omega_1 = 20$ meV with the coupling constant $\lambda_1 = 2.6$, another at $\hbar\omega_2 = 2100$ meV with the coupling constant $\lambda_2 = 0.3$. By solving the s-wave Eliashberg equations with the above spectral density, we find that $T_c = 106$ K for $\mu^* = 0.1$. In order to obtain $T_c = 105$ K with one δ -function, we need the following parameters: $\lambda_1 = 2.9$, $\hbar\omega_1 = 39.5$ meV, and $\mu^* = 0.1$. If we take $\mu^* = 0$, we need $\lambda_1 = 2.9$ and $\hbar\omega_1 = 33.6$ meV to have $T_c = 105$ K. Because we have used the δ -functions, the calculated T_c values should be the upper limits.

VIII. CONCLUSION

We have determined the polaron binding energy E_p for undoped parent cuprates from the unconventional oxygen-isotope effect on the antiferromagnetic ordering temperature (T_N). The deduced value (about 1.0 eV) of E_p is in quantitative agreement with that estimated from independent optical data and that estimated theoretically from the measured dielectric constants. The polaron binding energy should be large enough to overcome the intersite Coulomb interaction to form intersite bipolarons in deeply underdoped cuprates, in agreement with theory and experiment^{23,16}. The substantial oxygen-isotope effect on the in-plane supercarrier mass observed in optimally doped cuprates suggests that polarons are bound into the Cooper pairs. The bipolaron picture may be irrelevant for optimally doped cuprates because the

superconducting transition is of BCS-like. We also identify the phonon modes that are strongly coupled to conduction electrons from the angle-resolved photoemission spectroscopy (ARPES), tunneling spectra, and optical data. We consistently show that there is a very strong electron-phonon coupling feature at a phonon energy of about 20 meV along the antinodal direction and that this coupling becomes weaker towards the diagonal direction. We further show that high-temperature superconductivity in cuprates is caused by strong electron-phonon coupling, polaronic effect, and significant coupling with 2 eV Cu-O charge transfer fluctuation. The role of the antiferromagnetism in superconductivity appears to be insignificant because the antiferromagnetic and superconducting phases do not mix, as shown recently by Bozovic and coworkers⁷⁹.

* gzhao2@calstatela.edu

-
- ¹ J. G. Bednorz and K. A. Müller, *Z. Phys. B* **64**, 189 (1986).
² R. J. Cava, B. Batlogg, R. B. van Dover, D. W. Murphy, S. Sunshine, T. Siegrist, J. P. Remeika, E. A. Rietman, S. Zahurak, and G. P. Espinosa, *Phys. Rev. Lett.* **58**, 1676 (1987).
³ B. Batlogg, R. J. Cava, A. Jayaraman, R. B. van Dover, G. A. Kourouklis, S. Sunshine, D. W. Murphy, L. W. Rupp, H. S. Chen, A. White, K. T. Short, A. M. Mjuscce, and E. A. Rietman, *Phys. Rev. Lett.* **58**, 2333 (1987).
⁴ L. C. Bourne, M. F. Crommie, A. Zettl, H. zur Loye, S. W. Keller, K. L. Leary, A. M. Stacy, K. J. Chang, M. L. Cohen, and D. E. Morris, *Phys. Rev. Lett.*, **58**, 2337 (1987).
⁵ G. M. Zhao, K. K. Singh, and D. E. Morris, *Phys. Rev. B* **50**, 4112 (1994).
⁶ G. M. Zhao and D. E. Morris, *Phys. Rev. B* **51**, 16487R (1995).
⁷ G. M. Zhao, K. K. Singh, A. P. B. Sinha, and D. E. Morris, *Phys. Rev. B* **52**, 6840 (1995).
⁸ G. M. Zhao, M. B. Hunt, H. Keller, and K. A. Müller, *Nature (London)* **385**, 236 (1997).
⁹ G. M. Zhao, K. Conder, H. Keller, and K. A. Müller, *J. Phys.: Condens. Matter*, **10**, 9055 (1998).
¹⁰ R. J. McQueeney, Y. Petrov, T. Egami, M. Yethiraj, G. Shirane, and Y. Endoh, *Phys. Rev. Lett.* **82**, 628 (1999).
¹¹ A. Lanzara, G. M. Zhao, N. L. Saini, A. Bianconi, K. Conder, H. Keller, and K. A. Müller, *J. Phys.: Condens. Matter* **11**, L541 (1999).
¹² A. Shengelaya, G. M. Zhao, C. M. Aegerter, K. Conder, I. M. Savic, and H. Keller, *Phys. Rev. Lett.* **83**, 5142 (1999).
¹³ O. V. Misochko, E. Ya. Sherman, N. Umesaki, K. Sakai, S. Nakashima, *Phys. Rev. B* **59**, 11495 (1999).
¹⁴ J. Hofer, K. Conder, T. Sasagawa, G. M. Zhao, M. Willemin, H. Keller, and K. Kishio, *Phys. Rev. Lett.* **84**, 4192 (2000).
¹⁵ G. M. Zhao, H. Keller, K. Conder, *J. Phys.: Condens. Matter*, **13**, R569 (2001).
¹⁶ G. M. Zhao, *Phil. Mag. B* **81**, 1335 (2001).
¹⁷ G. M. Zhao, V. Kirtikar, and D. E. Morris, *Phys. Rev. B* **63**, 220506R (2001).
¹⁸ A. Lanzara, P. V. Bogdanov, X. J. Zhou, S. A. Kellar, D. L. Feng, E. D. Lu, T. Yoshida, H. Eisaki, A. Fujimori, K. Kishio, J.-I. Shimoyama, T. Nodak, S. Uchidak, Z. Hussain, and Z.-X. Shen, *Nature (London)* **412**, 510 (2001).
¹⁹ R. Khasanov, D.G. Eshchenko, H. Luetkens, E. Morenzoni, T. Prokscha, A. Suter, N. Garifanov, M. Mali, J. Roos, K. Conder, and H. Keller, *Phys. Rev. Lett.* **92**, 057602 (2004).
²⁰ X. J. Zhou, J. R. Shi, T. Yoshida, T. Cuk, W. L. Yang, V. Brouet, J. Nakamura, N. Mannella, Seiki Komiya, Yoichi Ando, F. Zhou, W. X. Ti, J. W. Xiong, Z. X. Zhao, T. Sasagawa, T. Kakeshita, H. Eisaki, S. Uchida, A. Fujimori, Zhenyu Zhang, E. W. Plummer, R. B. Laughlin, Z. Hussain, and Z.-X. Shen, *cond-mat/0405130*.
²¹ G. M. Zhao, K. Conder, H. Keller, and K. A. Müller, *Nature (London)* **381**, 676 (1996).
²² G. M. Zhao, H. Keller, R. L. Greene, and K. A. Müller, *Physics of Manganites*, edited by T. A. Kaplan and S. D. Mahanti (Kluwer Academic/Plenum publisher, New York, 1999) page 221.
²³ A. S. Alexandrov and N. F. Mott, *Polarons and Bipolarons* (World Scientific, Singapore, 1995).
²⁴ Z.-X. Shen, A. Lanzara, and N. Nagaosa, *cond-mat/0102244*.
²⁵ T. P. Devereaux, T. Cuk, Z.-X. Shen, and N. Nagaosa, *Phys. Rev. Lett.* **93**, 117004 (2004).
²⁶ G. M. Zhao, *Phys. Rev. B* **64**, 024503 (2001); G. M. Zhao, *cond-mat/0302566* (to be published in *Phil. Mag. B*); G. M. Zhao, *cond-mat/0305483* (to be published in *Phil. Mag. B*).
²⁷ B. H. Brandow, *Phys. Rev. B* **65**, 054503 (2002).
²⁸ X. X. Bi and P. C. Eklund, *Phys. Rev. Lett.* **70** 2625 (1993).
²⁹ A S Alexandrov and A M Bratkovsky, *J. Phys.: Condens. Matter* **11**, L531 (1999).
³⁰ T. Thio *et al.*, *Phys. Rev. B* **38**, 905 (1988).
³¹ J. H. Cho, F. C. Chou, and D. C. Johnston, *Phys. Rev. Lett.* **70**, 222 (1993).
³² I. Eremin, O. Kamaev, and M. V. Eremin, *Phys. Rev. B* **69**, 094517 (2004).
³³ M. Gruninger, D. van der Marel, A. Damascelli, A. Erb, T. Nunner, and T. Kopp, *Phys. Rev. B* **62**, 12422 (2000).
³⁴ J. D. Perkins, J. M. Graybeal, M. A. Kastner, R.J. Birgeneau, J. P. Falck, and M. Greven, *Phys. Rev. Lett.* **71**, 1621 (1993).
³⁵ H. S. Choi, E. J. Choi, and Y. J. Kim, *Physica C* **304**, 66 (1998).
³⁶ S. Uchida, T. Ido, H. Takagi, T. Arima, Y. Tokura, and S. Tajima, *Phys. Rev. B* **43**, 7942 (1991).
³⁷ J. P. Carbotte, *Rev. Mod. Phys.* **62**, 1027 (1990).
³⁸ A. S. Alexandrov, *Russ. J. Phys. Chem.* **57**, 167 (1983).
³⁹ A. S. Alexandrov, *Theory of superconductivity* (IoP Publishing, Bristol-Philadelphia, 2003).
⁴⁰ J. R. Shi S.-J. Tang, Biao Wu, P. T. Sprunger, W. L. Yang, V. Brouet, X. J. Zhou, Z. Hussain, Z.-X. Shen, Zhenyu

- Zhang, and E. W. Plummer, *Phys. Rev. Lett.* **92**, 186401 (2004)
- ⁴¹ P. D. Johnson, T. Valla, A.V. Fedorov, Z. Yusof, B. O. Wells, Q. Li, A. R. Moodenbaugh, G. D. Gu, N. Koshizuka, C. Kendziora, Sha Jian, and D. G. Hinks, *Phys. Rev. Lett.* **87**, 177007 (2001).
- ⁴² L. Buschmann, M. Boekholt, and G. Güntherodt, *Physica C* **203**, 68 (1992).
- ⁴³ Y. DeWilde, N. Miyakawa, P. Guptasarma, M. Iavarone, L. Ozyuzer, J.F. Zasadzinski, P. Romano, D.G. Hinks, C. Kendziora, C.W. Crabtree, and K.E. Gray, *Phys. Rev. Lett.* **80**, 153 (1998).
- ⁴⁴ L. Ozyuzer, J.F. Zasadzinski, C. Kendziora, and K. E. Gray, *B* **61**, 3629 (2000).
- ⁴⁵ S. Sinha and K.-W. Ng, *Phys. Rev. Lett.* **80**, 1296 (1998).
- ⁴⁶ L. Alff, A. Beck, R. Gross, A. Marx, S. Kleefisch, Th. Bauch, H. Sato, M. Naito, and G. Koren, *Phys. Rev. B* **58**, 11197 (1998).
- ⁴⁷ K. C. Hewitt, T. P. Devereaux, X. K. Chen, X-Z Wang, J. G. Naeni, A. E. Curzon, and J. C. Irwin, *Phys. Rev. Lett.* **78**, 4891 (1997).
- ⁴⁸ A. Sacuto, R. Combescot, N. Bontemps, P. Monod, V. Viallet, and D. Colson, *Europhys. Lett.* **39**, 207 (1997).
- ⁴⁹ T. P. Devereaux, *Phys. Rev. Lett.* **74**, 4343 (1995).
- ⁵⁰ P. J. Hirschfeld and N. Goldenfeld, *Phys. Rev. B* **48**, 4219 (1993).
- ⁵¹ J. Le Cochea, G. Lamuraa, A. Gauzzib, F. Liccib, A. Revcolevschic, A. Erbd, G. Deuschere and J. Boka, *cond-mat/0001045*.
- ⁵² A. D. Gromko, A. V. Fedorov, Y.-D. Chuang, J. D. Koralek, Y. Aiura, Y. Yamaguchi, K. Oka, Yoichi Ando, and D. S. Dessau, *Phys. Rev. B* **68**, 174520 (2003).
- ⁵³ M. Eschrig and M. R. Norman, *Phys. Rev. Lett.* **89**, 277005 (2002).
- ⁵⁴ H. Ding, J.C. Campuzano, A.F. Bellman, T. Yokoya, M.R. Norman, M. Randeria, T. Takahashi, H. Katayama-Yoshida, T. Mochiku, K. Kadowaki, and G. Jennings, *Phys. Rev. Lett.* **74**, 2784 (1995).
- ⁵⁵ R. S. Gonnelli, G. A. Ummarino, and V. A. Stepanov, *Physica C* **275**, 162 (1997).
- ⁵⁶ W. E. Pickett, R. E. Cohen, and H. Krakauer, *Phys. Rev. Lett.* **67**, 228 (1991).
- ⁵⁷ H. He, Y. Sidis, P. Bourges, G. D. Gu, A. Ivanov, N. Koshizuka, B. Liang, C. T. Lin, L. P. Regnault, E. Schoenher, and B. Keimer, *Phys. Rev. Lett.* **86**, 1610 (2001)
- ⁵⁸ J. P. Carbotte, E. Schachinger, and D. N. Basov, *Nature (London)* **401**, 354 (1999).
- ⁵⁹ E. Schachinger and J. P. Carbotte, *Phys. Rev. B*, **62**, 9054 (2000).
- ⁶⁰ F. Marsiglio, T. Startseva, and J.P. Carbotte, *Physics Lett. A* **245**, 172 (1998).
- ⁶¹ J. Orenstein, *Nature (London)* **401**, 333 (1999).
- ⁶² V. M. Krasnov, A. Yurgens, D. Winkler, P. Delsing, and T. Claeson, *Phys. Rev. Lett.* **84**, 5860 (2000).
- ⁶³ M. Opel M. Opel and R. Hackl, D- T. P. Devereaux, A. Virosztek, A. Zawadowski, A. Erb, E. Walker, H. Berger, and L. Forro, *Phys. Rev. B* **60**, 9836 (1999).
- ⁶⁴ C. O. Rodriguez, A. I. Liechtenstein, I. I. Mazin, O. Jepen, O. K. Anderson, M. Methfessel, *Phys. Rev. B* **42**, 2692 (1990).
- ⁶⁵ N. Miyakawa, P. Guptasarma, J. F. Zasadzinski, D. G. Hinks, and K. E. Gray, *Phys. Rev. Lett.* **80**, 157 (1998).
- ⁶⁶ A. Abanov, A. V. Chubukov, and J. Schmalian, *Phys. Rev. B* **63**, 180510R (2001).
- ⁶⁷ J. Hwang, T. Timusk, and G. D. Gu, *Nature (London)* **427**, 714 (2004).
- ⁶⁸ I. Vobornik, R. Gatt, T. Schmauder, B. Frazer, R. J. Kelley, C. Kendziora, M. Grioni, M. Onellion, and G. Margaritondo, *Physica C* **317-318**, 589 (1999).
- ⁶⁹ S. V. Borisenko, A. A. Kordyuk, T. K. Kim, A. Koitzsch, M. Knupfer, J. Fink, M. S. Golden, M. Eschrig, H. Berger, and R. Follath, *Phys. Rev. Lett.* **90**, 207001 (2003).
- ⁷⁰ G.A. Ummarino, R.S. Gonnelli, and D. Daghero, *Physica C* **377**, 292 (2002).
- ⁷¹ J.F. Zasadzinski, L. Coffey, P. Romano and Z. Yusof, *Phys. Rev. B* **68**, 180504 (2003).
- ⁷² L. Ozyuzer, J. F. Zasadzinski, N. Miyakawa *Int. J. Mod. Phys. B* **29-31**, 3721 (1999).
- ⁷³ H. Hancotte, R. Deltour, D. N. Davydov, A. G. M. Jansen, and P. Wyder, *Phys. Rev. B* **55**, R3410 (1997).
- ⁷⁴ M. J. Holcomb, J. P. Collman, and W. A. Little, *Phys. Rev. Lett.* **73**, 2360 (1994).
- ⁷⁵ M. J. Holcomb, C. L. Perry, J. P. Collman, and W. A. Little, *Phys. Rev. B* **53**, 6734 (1996).
- ⁷⁶ M. Gulacsi and R. J. Chan, *J. Supercond.* **14**, 651 (2001), and private communication with M. Gulacsi.
- ⁷⁷ M. A. Quijada, D. B. Tanner, R. J. Kelley, M. Onellion, H. Berger, and G. Margaritondo, *Phys. Rev. B* **60**, 14 917 (1999).
- ⁷⁸ V. Z. Kresin, *Phys. Lett. A* **122**, 434 (1987).
- ⁷⁹ I. Bozovic, G. Logvenov, M. A. J. Verhoeven, P. Caputo, E. Goldobin, and T. H. Geballe, *Nature (London)* **442**, 873 (2003).